Journal of Advanced Research in Applied Sciences and Engineering Technology

Journal homepage:
https://semarakilmu.com.my/journals/index.php/applied_sciences_eng_tech/index
ISSN: 2462-1943

Mineralogical Analysis of Lithomargic Clay Deposits along the Coastal Belt of Uttara Kannada Region in South India

Deepak Nayak[1], Purushotham G. Sarvade[1,*], Udaya Shankara H. N.[1], M. Prasanna Kumar[1]

[1] Department of Civil Engineering, Manipal Institute of Technology, Manipal Academy of Higher Education, Manipal 576104, Karnataka, India

ARTICLE INFO

Article history:
Received 7 August 2023
Received in revised form 26 November 2023
Accepted 22 December 2023
Available online 7 February 2024

Keywords:

Lithomargic clay; Mineral compounds; XRD analysis; Elements

ABSTRACT

The Lithomargic clay, generally known as Shedi soil found below the lateritic soil along the coastal belt of Karnataka. This lithomargic clay is rich in silt content and dispersive in nature. The dispersion or de-flocculation behaviour of clays is influenced by factors including mineral composition, soil chemistry, the presence of dissolved salts in the pore water, and the characteristics of the erosive water. This type of soil is liable to erosion and landslides. At present, coastal belt of Uttara Kannada district is witnessing a lot of developments in terms of Industry, infrastructures, and other activities. Lithomargic clay represents a challenging soil variety that necessitates comprehensive examination to render it compatible for supporting various engineering structures such as buildings, pavements, railways, and dam. The X-ray diffraction and Energy Dispersive X-Ray Spectroscopy (EDS) analysis were conducted to identify the presence of minerals and compounds for the various soil samples collected along the coastal belt of Uttara Kannada District. The minerals observed in most of the locations are quartz, feldspar like orthoclase, microcline, albite, mica group consisting of muscovite and biotite, those that are not altered chemically since the time of formation and deposition. The presence of secondary minerals like kaolinite, illite, montmorillonite, vermiculite, gibbsite, and calcite are witnessed by the X-ray diffraction analysis.

1. Introduction

The lithomargic clay, commonly referred to as shedi soil in the local context, is typically located beneath the lateritic soil. It forms a significant part of silt deposits and is known for its dispersive characteristics, making it susceptible to erosion. This clay is predominantly present along the western coast of South India. In India, it is commonly observed at depths ranging from one to three meters beneath the uppermost layer of lateritic soil along the western coastal zones, extending from Trivandrum to Mumbai, and in areas connecting the Deccan Plateau [1,2]. It is formed due to tropical or subtropical weathering, which contains hydrated alumina, kaolinite, and primary silicates. It also has an amorphous blend of $Al_2Si_2O_5(OH)_4$ [3]. The investigation into lithomargic clay along the Udupi region's coastal belt revealed abundant minerals, including quartz, feldspar (such as orthoclase),

* *Corresponding author.*
E-mail address: pg.sarvade@manipal.edu

https://doi.org/10.37934/araset.39.1.117134

muscovite, kaolinite, dickite, gibbsite, halloysite and illite in substantial proportions [4]. This distinctive residual soil, known as lithomargic clay, displays a pinkish and whitish coloration and is predominantly composed of illite and kaolinite. The weathering of laterite soils in tropical and subtropical regions leads to its production [5]. Several factors like soil chemistry, eroding water, and mineralogy, influence the dispersion behaviour of lithomargic clays. In experiments, blending the soil with lime in concentrations of 2%, 4%, and 6% resulted in a noteworthy reduction in the dispersion of lithomargic clay, reaching 12.9% with the addition of 6% lime [6]. Notably, incorporating randomly distributed coir reinforcement led to a significant increase in strength [7]. The coir embedded mat reinforcement to lithomargic clay contributed to the improvement of strength [8].

The main types of iron found below the ferruginous zone were hematite or goethite, while the main types of aluminium found below the ferruginous zone were kaolinite or gibbsite. Based on their mineralogy, these deposits are classified as lithomargic clay, ferruginous laterites, and aluminous laterites. Major mineral transformations, such as the alteration of feldspar into montmorillonite, illite, kaolinite, or halloysite, and ultimately bauxite, occur during the in-situ production of laterites from parent rocks with granite or granitic gneiss compositions [9].

The best results were obtained by combining 25% granulated blast furnace slag (GBFS) with lithomargic clay. Addition of 2% and 4% cement to the optimized mix also improved the situation. The strength gain was supported by SEM and XRD study, which linked it to substances such calcium silicate hydroxide hydrate (CSHH), calcium aluminate silicate hydrates (C-A-S-H), and related substances [10]. Gibbsite, muscovite, kaolinite and biotite were among the minerals found in lithomargic clay according to XRD study [11]. Laita *et al*., [12] examined how the physical characteristics of the materials were affected by mineralogical and textural changes in bauxite with illite- and kaolinite-rich clays flamed between 1000 and 1270 °C. The creation of a Si and Al-rich vitreous phase and the subsequent crystallization of cristobalite, ilmenite, hercynite, mullite, and corundum at high temperatures resulted from the production of mullite at 1000 degrees Celsius. Bhat and Nayak [13] conducted experiments to enhance the strength properties of lithomargic clay through chemical stabilization by the mix of lime and granulated blast furnace slag (GBFS). Addressing the environmental concern of disposing of significant volumes of industrial waste, namely GBFS, the study proposed its utilization for long-term soil stabilization. Laboratory investigations were carried out on lithomargic clay, replacing variable proportions with GBFS and incorporating different lime percentages to optimize lime usage and elucidate the strength enhancement process. The optimal combination of lime and GBFS was identified as 4% and 20%, respectively. Substantial improvement in strength was achieved when lithomargic clay was blended with 20% GBFS and 4 % lime. SEM and XRD analyses of the stabilized soil revealed structural changes and witnessed the formation of compounds such as CASH, CSHH, CAOH, gyrolite, and gismondine [13].

Narloch *et al*., [14] examined the influence of mineral composition on the compressive strength of cement-stabilized rammed earth (CSRE). Compression tests were conducted on CSRE samples with varied mineral compositions while maintaining consistent particle size distribution, cement content, and water content. The study found that changes in mineral composition altered the compressive strength of CSRE. Montmorillonite substantially reduced compressive strength, while beidellite had a lesser impact, and kaolinite moderately increased compressive strength.

The unconfined compressive strength (UCS) and the California bearing ratio (CBR) increased when GGBS and fly ash were added to the soil at replacement ratios of 20%, 30%, and 40%. In the meantime, different sodium oxide doses of 2%, 3%, and 4% were added while maintaining a consistent weight-to-volume ratio of 1.25 for the silica oxide to sodium oxide solution [15]. Upon stabilizing lithomargic clay with cement, XRD analysis indicated the formation of ettringite, calcium silicate hydrate (CSH), and calcium aluminate hydrate (CAH). The SEM study demonstrated

alterations in the soil's structure due to the additions of cement and quarry dust [16]. In a mineralogical study by Bhagyashree *et al*., [17] on lateritic soil situated above lithomargic clay, observed minerals included Corundum, Anatase, Magnetite, Quartz, and Hematite. Contaminants impact the engineering and chemical characteristics of soil, leading to a decrease in both its overall strength and, consequently, its suitability as a foundation material [18]. In potassium hydroxide (KOH) medium, the reaction products formed in red earth are mainly muscovite [19].

Understanding the minerals within the soil is crucial for comprehending the physical and chemical behaviour of the soil. It is essential to identify the minerals present and their variations across the study area. By gaining insights into the characteristics and behaviour of these minerals, one can determine appropriate ground improvement techniques to address soil deficiencies. In this study, we assess the characterization and mineralogical properties using X-ray diffraction (XRD), energy dispersive X-ray spectroscopy (EDS), and scanning electron microscopy (SEM) analyses on soil samples collected from the coastal belt of Uttara Kannada regions of South India. This aids in establishing correlations between mineralogy and geotechnical parameters, ultimately guiding the recommendation of suitable ground improvement techniques for the soil in future.

2. Methodology

2.1 Identification and Collection of Soil Sample

Lithomargic clay, discovered beneath lateritic soils, exhibits whitish, yellowish, and pinkish hues and is classified as silty sand. This study involves the collection of soil samples from the coastal belt of Uttara Kannada district. To precisely characterize the properties of lithomargic clay, soil samples were collected from various locations along the coastal belt of Uttara Kannada district, specifically from Shiroor, Behalli, Shirali, Bhatkal, Ternamakki, Tumbebeela, Honnavar, Manki, Haladipur, and Kumta.

2.2 Characterization of Lithomargic Clay in the Coastal Belt of Uttara Kannada District

2.2.1 Mineralogical tests

The mineralogical analysis comprises scanning electron microscopy (SEM) and energy dispersive X-ray spectroscopy (EDS), which are employed to ascertain the mineralogical composition. Soil samples, dried in an oven and passing through a 75 µ sieve, are utilized for conducting these mineralogical tests. Before the tests, gold sputtering is necessary over the soil surface. The outcomes obtained are then scrutinized to identify the elemental constituents within the soil.

2.2.2 Scanning electron microscopy (SEM) and energy dispersive x-ray spectroscopy (EDS)

Soil that has passed through a 75 µ sieve is gathered, and gold sputtering is applied to the sample. Subsequently, scanning electron microscopy is employed to examine the microstructure of the soil sample. The chemical composition of the specimen is then analysed using energy dispersive X-ray spectroscopy (EDS), which allows for the study and quantification of the elements. Scanning electron microscope (SEM) analysis was carried out using Zeiss EVO 18-EDX special edition machine compatible with EDX machine.

2.2.3 X-ray diffraction (XRD) analysis

Soil that has passed through a 425 µ sieve is gathered specifically for XRD analysis. X-ray diffraction (XRD) analysis was done using Cu-Kα radiation (k = 1.54 Å) at 40kV Rigaku MiniFlex 600 X-ray diffractometer. This analysis is conducted to determine the minerals present in the soil samples.

3. Results and Discussion

3.1 Mineralogical Tests

The elemental structure and minerals contained in the soil are analyzed using Scanning Electron Microscopy (SEM), which provides a microscopic image of the soil. Microfabric and mineralogical tests are then conducted on the soil samples. To ascertain the composition of the soil samples, Energy Dispersive X-Ray Spectroscopy (EDS) was used on them. Below are the findings from the mineralogical and microfabric tests that were done on the soil. The elements Oxygen(O), Aluminium (Al), Silicon (Si), Potassium(K), Sodium (Na), Calcium (Ca), Iron(Fe) and Magnesium(Mg) were found in the soil samples. The percentage of elements in terms of weights and corresponding atomic percentage of same elements observed in spectrum 1 and spectrum 2 are tabulated for various samples collected. The findings, which are displayed below, display the soil sample SEM pictures and EDS

3.1.1 Mineralogical analysis of Shiroor sample

As per quantification of results, as in Figure 1(d), it can be observed that the soil sample contains relatively larger percentage of microcline ($KAlSi_3O_8$) (21%), illite ($K_4Al_{16}Si_8O_{48}$) (11%), muscovite ($K_4Si_{12}.Al_{12}O_{48}$) (11%), kaolinite ($Al_2Si_2O_9H_4$) (10%), biotite ($Mg_4Al_4K_2Si_6O_{24}$) (8%) and vermiculite ($Mg_{5.35}Fe_{0.96}Al_{2.88}Si_{5.44}O_{36}$) (8%). The quartz ($Si_6O_6$) (1%), forsterite ($Mg_{4.28}Fe_{3.65}Mn_{0.05}Ca_{0.02}Si_4O_{16}$) (2%), alumina ($Al_2O_3$) (1%), mullite ($Al_{4.8}Si_{1.20}O_{9.6}$) (2%), calcite ($CaCO_3$) (1%) is found with low proportions. The montmorillonite ($Si_{7.8}Al_{1.72}Cs_{0.16}Fe_{0.20}Mg_{0.28}O_{20}$) is not showing a proper peak intensity. The SEM image from Figure 1(a) showing sheet mineral can be identified as vermiculite or biotite as EDS analysis confirm the presence of magnesium with potassium, alumina and silicates.

The elements found by the EDS analysis, which are listed in Table 1, and the spectrum image in Figure 1(b) make the compounds shown in the XRD analysis visible in Figure 1(c). The Table 1 represents the elements observed in spectrum 1 and spectrum 2 with their percentage weights of Shiroor sample. Iron, magnesium, potassium, and oxygen make up the majority of the elements found, followed by silicates, aluminium, and oxygen. Microcline and other potassium-based chemicals are present in significant amounts in this sample. Magnesium compounds are present in trace amounts. Iron oxide, forsterite, biotite, and vermiculite are all confirmed to exist by the presence of both the elements Fe and Mg. In the XRD examination, the minerals quartz, orthoclase, illite, and microcline can all be seen clearly.

Table 1
Elemental composition of Shiroor sample

Elements	C	O	Mg	Al	Si	K	Fe	C	O	Mg	Al	Si	K	Fe
	Weight (%)							Atomic Weight (%)						
Spectrum 1	35.52	40.3	0.22	9.12	9.3	0.83	4.71	47.24	40.24	0.15	5.4	5.29	0.34	1.35
Spectrum 2	-	58.34	0.07	17.82	22.29	1.49	-	-	70.93	0.05	12.84	15.44	0.74	-

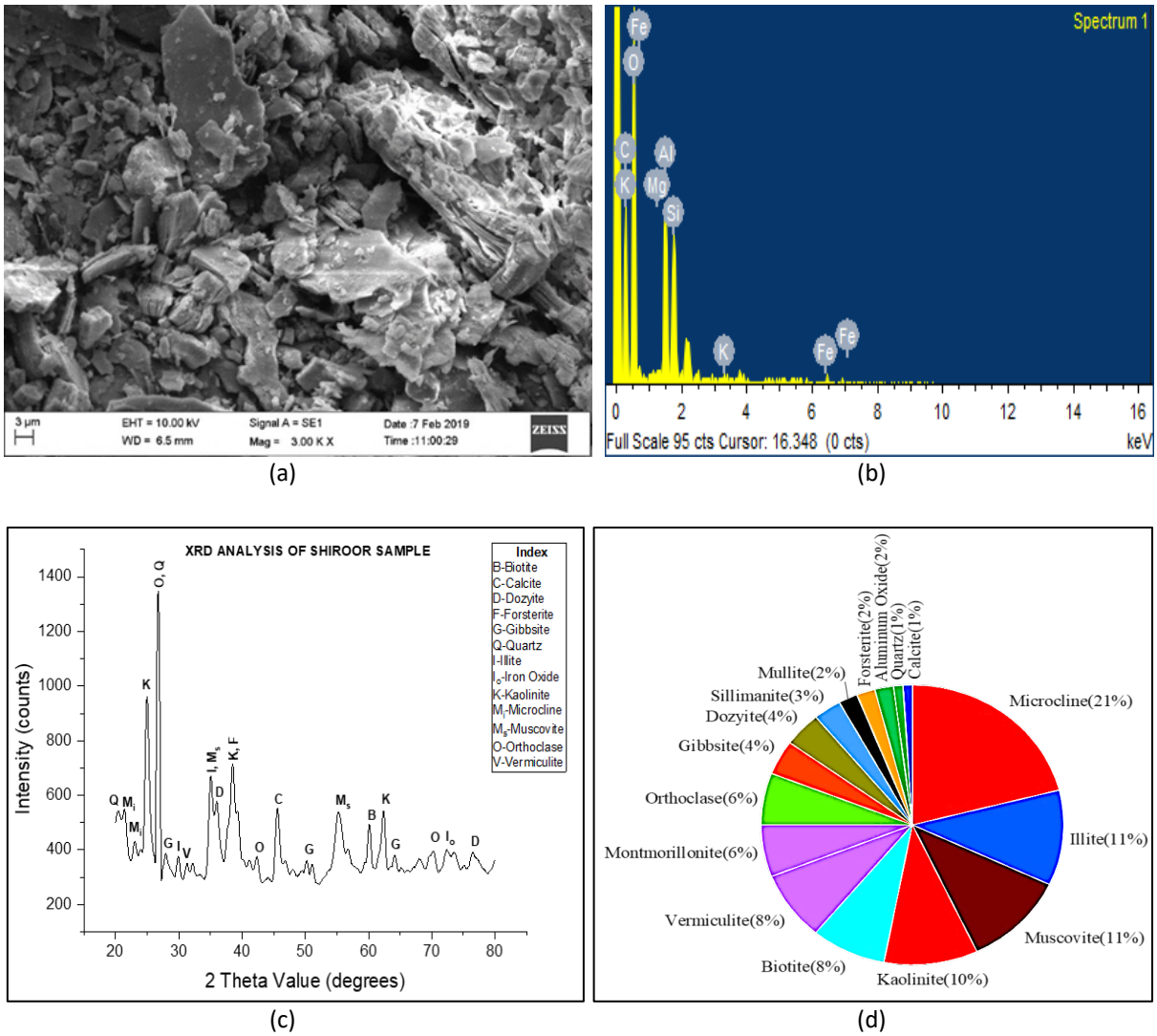

Fig. 1. Shiroor sample (a) SEM image (b) Spectrum image (c) XRD analysis (d) Quantification of compounds

2.1.2 Mineralogical analysis of Behalli sample

The SEM image in Figure 2(c) can be identified as illite due to the presence of lath to fibre shaped crystals [20]. The Figure 2(b) shows the EDS spectrum of the Behallli sample depicting the elements observed in the Behalli sample. The elements like aluminium, silica, iron, magnesium, potassium, carbon and oxygen are witnessed by EDS analysis. The Weight percentage and atomic percentages of all elements observed are as shown in Table 2 and confirm the presence of compounds identified.

Table 2
Elemental composition of Behalli sample

Elements	C	O	Mg	Al	Si	K	Fe	C	O	Mg	Al	Si	K	Fe
	Weight (%)							Atomic Weight (%)						
Spectrum 1	15.14	55.37	0.01	14.04	14.27	1.17	-	21.81	59.87	0.01	9	8.79	0.52	-
Spectrum 2	-	55.59	-	19.49	23.13	0.86	0.92	-	68.68	-	14.27	16.28	0.44	0.33

The Figure 2(c) shows the XRD analysis of Behalli sample. The XRD analysis depicts the minerals like kaolinite ($Al_2Si_2O_9H_4$), illite ($K_4Al_{16}Si_8O_{48}$), gibbsite ($Al_8O_{24}H_{24}$) microcline ($KAlSi_3O_8$), muscovite ($K_4Si_{12}.Al_{12}O_{48}$), quartz (Si_6O_6), sillimanite ($Al_8Si_4O_{20}$), biotite ($Mg_4Al_4K_2Si_6O_{24}$), forsterite ($Mg_{4.28}Fe_{3.65}Mn_{0.05}Ca_{0.02}Si_4O_{16}$), dozyite ($Mg_{18}O_{54}Si_{12}$), orthoclase ($K_4A_{l4}Si_{12}O_{32}$), vermiculite ($Mg_{5.35}Fe_{0.96}Al_{2.88}Si_{5.44}O_{36}$), calcite (CaCO3), mullite ($Al_{4.8}Si_{1.20}O_{9.6}$), iron oxide (Fe_2O_3), alumina (Al_2O_3).

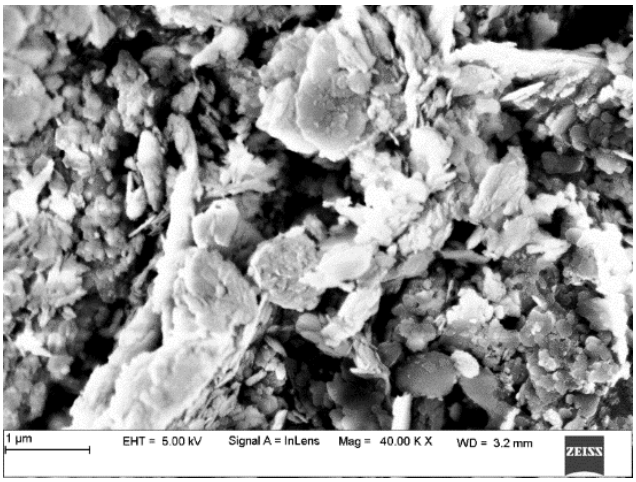

(a)

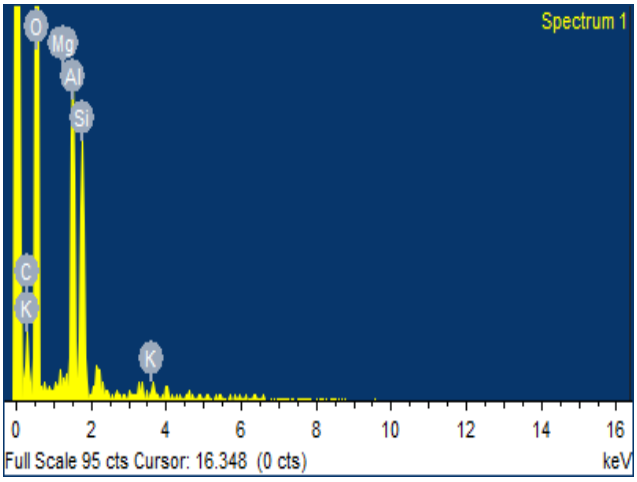

(b)

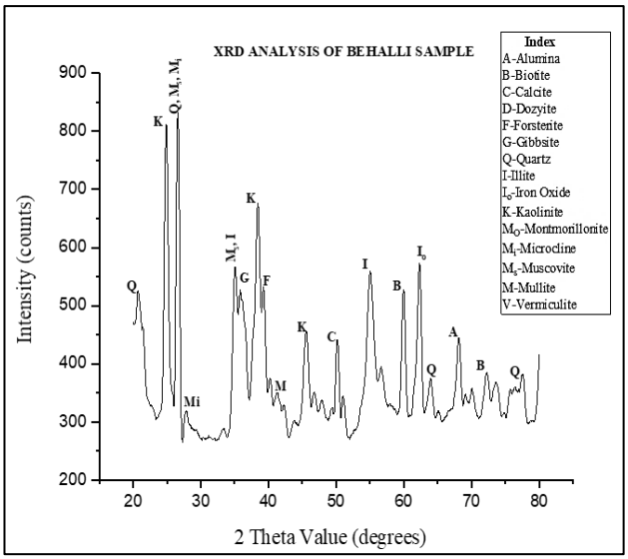

(c)

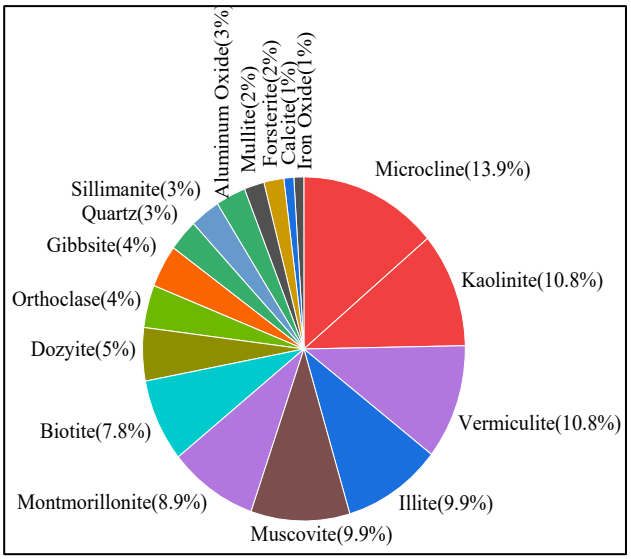

(d)

Fig. 2. Behalli sample (a) SEM image (b) Spectrum image (c) XRD analysis (d) Quantification of compounds

As per quantification of results from Figure 2(d), it is found that the soil sample includes relatively higher proportions of microcline (13.9%), kaolinite (10.8%), vermiculite (10.8%), illite (9.9%) and muscovite (9.9%). The quartz (3%), sillimanite (3%), alumina (2%), mullite (2%), forsterite (2%), iron oxide (1%) and calcite (1%) are present at very less proportions. The minerals identified in the XRD analysis are confirmed by the EDS analysis as listed in Table 2. Most of the elements observed are oxygen, silicates and aluminium followed by carbon and potassium.

2.1.3 Mineralogical analysis of Bhatkal sample

The microscopic image can be observed in Figure 3(a). As per quantification of results, as depicted by Figure 3(d), the soil sample includes relatively higher proportions of vermiculite (15.3%), kaolinite (14.3%), microcline (13.3%), illite (12.2%) and muscovite (8.2%). The quartz (2%), sillimanite (2%), alumina (2%), mullite (2%), forsterite (2%), iron oxide (0.3%) and calcite (2%) are present at less proportions.

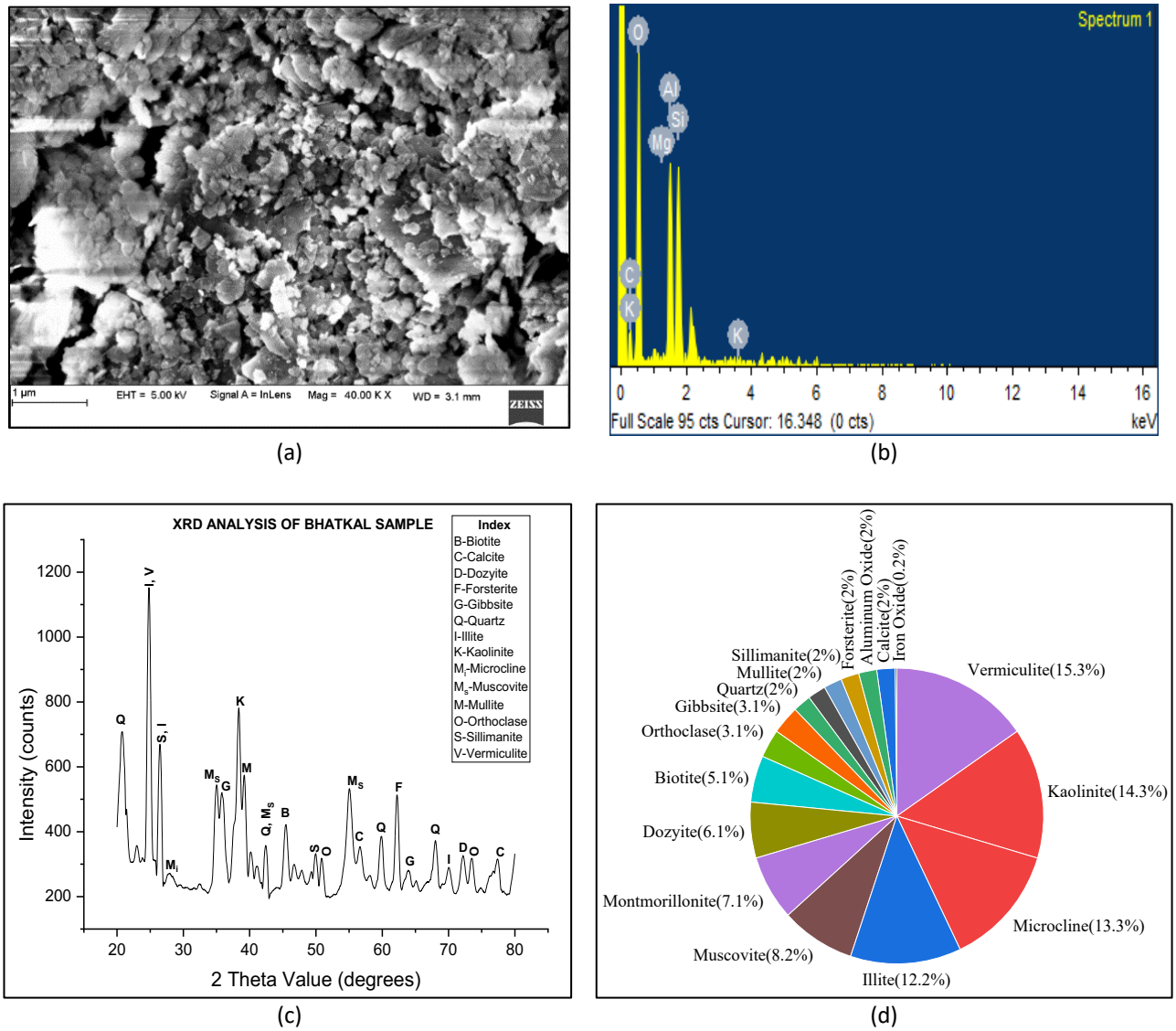

Fig. 3. Bhatkal sample (a) SEM image (b) Spectrum image (c) XRD analysis (d) Quantification of compounds

The compounds identified by XRD analysis as shown in Figure 3(c) are evident from the elements observed by the EDS analysis as listed in Table 3. Most of the elements observed are oxygen, silicates and aluminium followed by carbon, magnesium and potassium. The vermiculites are believed to be formed from weathering of biotite and its presence can be witnessed in the XRD analysis. The main elements of these compounds like aluminium, silica, iron and magnesium are clearly evident from the EDS analysis as shown in Table 3 and observed in Figure 3(b). Illite, muscovite and microcline can also be observed to be relatively at large proportions. Illite is considered to be weathering product of microcline and muscovite feldspar. The EDS analysis also confirms the presence of elements of Illite, muscovite and microcline.

Table 3
Elemental composition of Bhatkal sample

Elements	C	O	Mg	Al	Si	K	Fe	C	O	Mg	Al	Si	K	Fe
	Weight (%)							Atomic Weight (%)						
Spectrum 1	10.61	48.89	0.14	17.21	22.3	0.85	-	16.36	56.6	0.11	11.81	14.71	0.4	-
Spectrum 2	-	53.38	-	19.24	18.39	1.04	7.95	-	68.47	-	14.64	13.43	0.54	2.92

2.1.4 Mineralogical analysis of Shirali soil sample

As per quantification of results, as in Figure 4(d), it can be observed that the soil sample contains larger proportions of microcline (12.1%), orthoclase (11.1%), vermiculite (10.1%), illite (9.1%) and kaolinite (9.1%). The quartz (1%), forsterite (3%) and alumina (2%) are present at less proportions. The gibbsite, microcline, orthoclase, kaolinite, forsterite and montmorillonite compounds are showing a proper peak intensity in XRD analysis as shown in Figure 4(c).

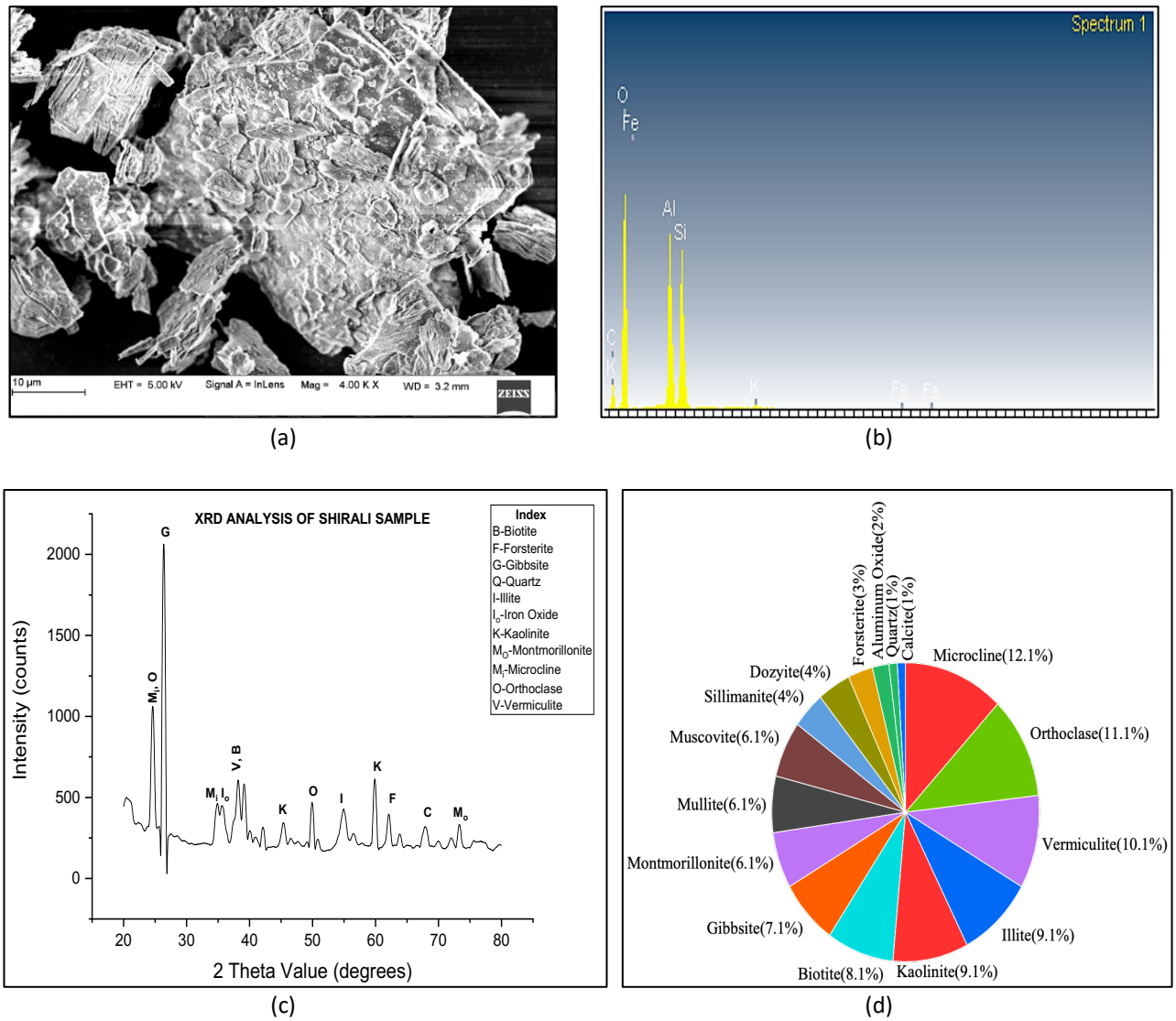

Fig. 4. Shirali sample (a) SEM image (b) Spectrum image (c) XRD analysis (d) Quantification of compounds

The elements found by the EDS analysis, which are listed in Table 4 and shown in Figure 4(b), clearly show the compounds found in the XRD study. Oxygen, silicates, and aluminium make up the majority of the elements found, with potassium, iron, and carbon coming in second. Large concentrations of silicate-based compounds such as microcline, orthoclase, illite, and kaolinite, as well as potassium and alumina, are present in this sample. Based on Suzuki *et al*., [21], observation of the pseudo-hexagonal platelets laminar structure and based on elemental analysis, the mineral depicted in Figure 4(a) of the SEM image can be recognized as gibbsite and kaolinite.

Table 4
Elemental composition of Shirali sample

Elements	O	Mg	Al	Si	Fe	K	O	Mg	Al	Si	Fe	K
	Weight (%)						Atomic Weight (%)					
Spectrum 1	55.6	0.81	14.54	22.4	6.65	-	70	0.67	10.86	16.07	2.4	-
Spectrum 2	64.75	0.5	14.01	19.51	-	1.22	76.17	0.39	9.77	13.08	-	0.59

2.1.5 Mineralogical analysis of Tumbebeela soil sample

As per quantification of results from Figure 5(d), it is found that the soil shows larger proportions of gibbsite (15.2%), illite (14.1%), microcline (10.1%), kaolinite (8.1%) and muscovite (8.1%). The forsterite (1%), mullite (1%) and alumina (2%) are present at lower proportions. The quartz is present at 5%, which is found to be relatively high compared to other samples. The quartz, illite, gibbsite, microcline, orthoclase and forsterite compounds are showing a proper peak intensity in XRD analysis. The minerals of SEM image as in Figure 5(a) showing irregular grain sizes with distinct separation to each other can be identified as forsterite and biotite [22].

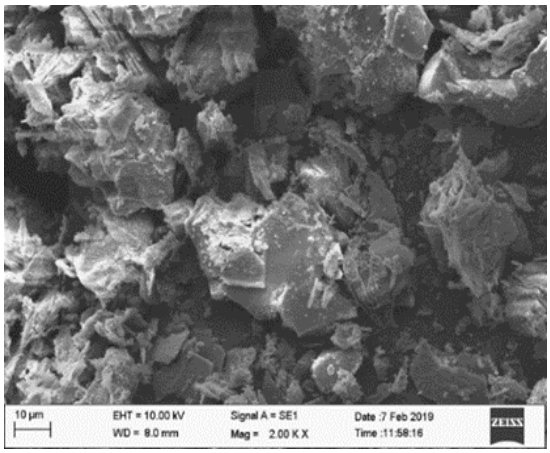

(a)

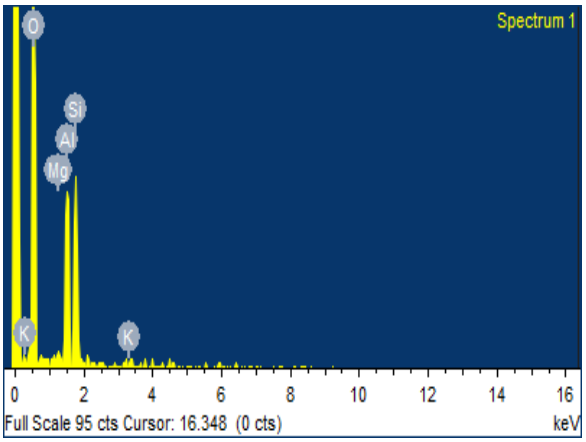

(b)

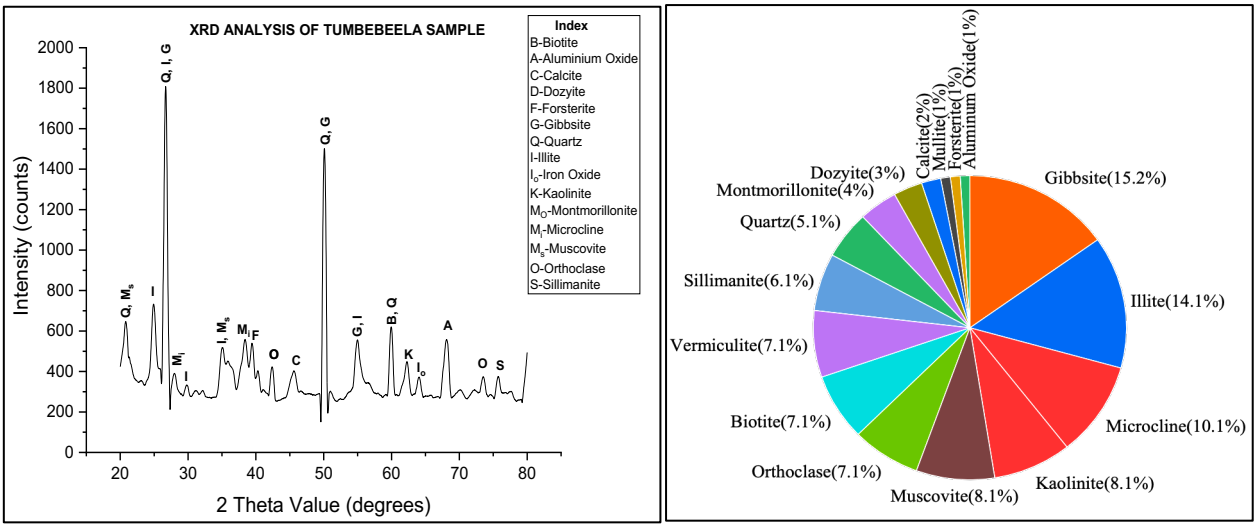

(c) (d)

Fig. 5. Tumbebeela sample (a) SEM image (b) Spectrum image (c) XRD analysis (d) Quantification of compounds

The compounds identified in XRD analysis (as depicted in Figure 5(c)) are evident from the EDS analysis as listed in Table 5 and spectrum image Figure 5(b). Most of the elements observed are oxygen, aluminium, potassium, silicates and iron. In this sample the potassium, alumina, silicate and magnesium-based compounds like gibbsite, microcline, orthoclase, illite and kaolinite are found in large proportions. The magnesium-based compounds like vermiculite, biotite and dozyite are found at low proportions and are confirmed by the EDS test.

Table 5
Elemental composition of Tumbebeela sample

Elements	C	O	Mg	Al	Si	K	Fe	C	O	Mg	Al	Si	K	Fe
	Weight (%)							Atomic Weight (%)						
Spectrum 1	14.61	46.49	0.29	14.39	16.52	1.1	6.6	22.52	53.79	0.22	9.87	10.89	0.52	2.19
Spectrum 2	-	52.97	0.16	15.26	21.99	1.45	8.17	-	68.28	0.13	11.66	16.14	0.77	3.02

2.1.6 Mineralogical analysis of Ternamakki soil sample

From the SEM image as in Figure 6(a), the minerals having lath to fibre shaped crystals identified as illite [20]. The quantification results from Figure 6(d), shows relatively higher proportions of microcline (14.9%), illite (13.9%), gibbsite (13.9%), muscovite (10.9%), orthoclase (6.9%) and sillimanite (6.9%) as depicted by quantification of compounds. The quartz (4%), forsterite (1%), alumina (2%), mullite (2%), kaolinite (2%), vermiculite (0.3%) and biotite (5%) are present at lesser proportions. The montmorillonite, vermiculite, biotite is not showing a proper peak intensity.

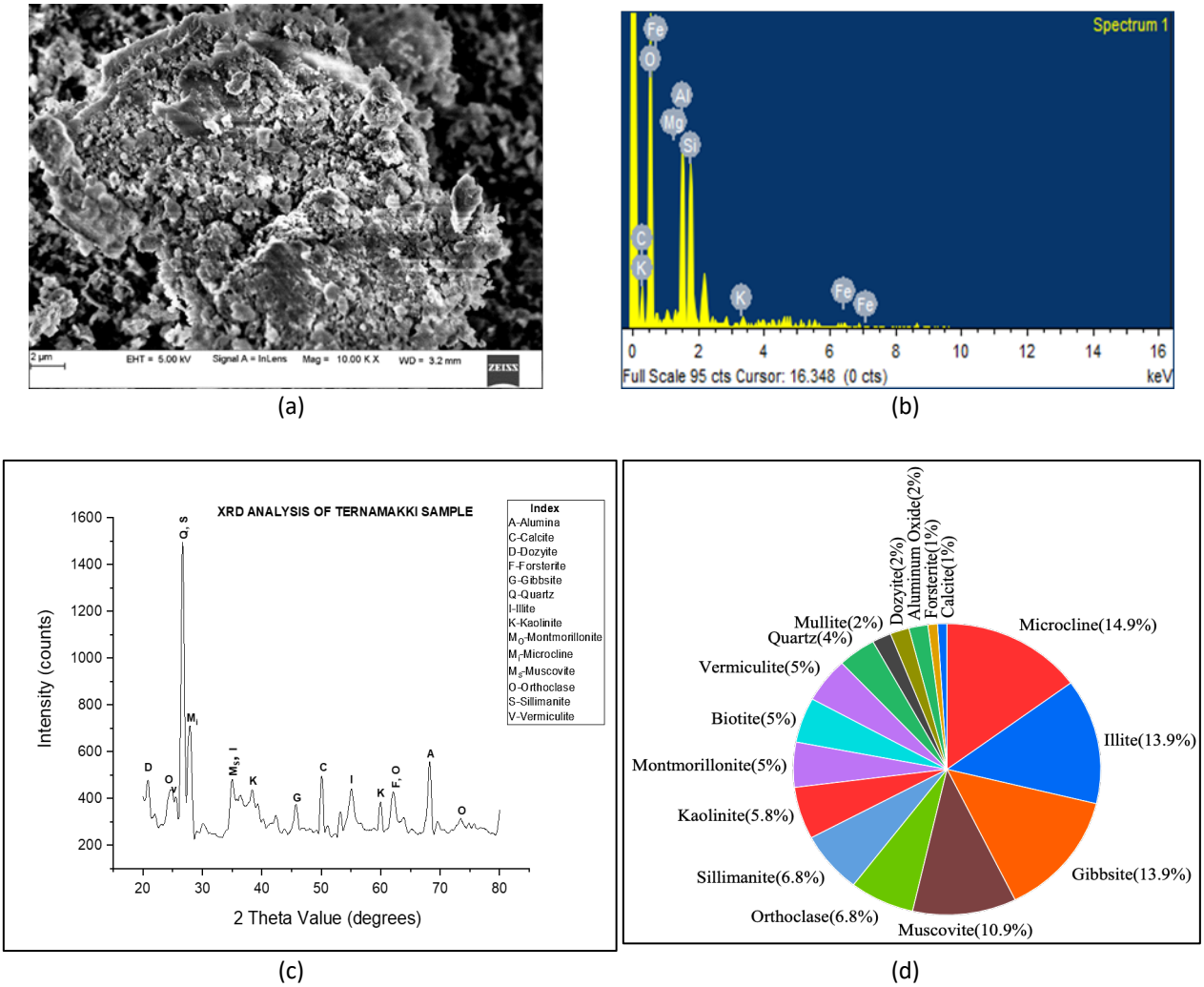

(a) (b) (c) (d)

Fig. 6. Ternamakki sample (a) SEM image (b) Spectrum image (c) XRD analysis (d) Quantification of compounds

The compounds observed in the XRD analysis (Figure 6(c)) are evident from the elements detected by the EDS analysis as listed in Table 6 and depicted in spectrum image Figure 6(b). Most of the elements observed are oxygen, silicates and aluminium followed by potassium. In this sample the potassium-based compounds like microcline are found in higher proportions. Magnesium compounds are found at in lower proportions. The presence of both elements Fe and Mg also confirms the presence of forsterite and vermiculite. The quartz, sillimanite and microcline minerals can be seen at high intensity in the XRD analysis.

Table 6
Elemental composition of Ternamakki sample

Elements	O	Mg	Al	Si	K	Fe	C	O	Mg	Al	Si	K	Fe	C
	Weight (%)							Atomic Weight (%)						
Spectrum 1	61.64	-	14.26	15.33	0.57	0.94	23.14	55.96	-	7.68	7.93	0.21	0..24	27.98
Spectrum 2	69.65	-	16.14	17.37	0.78	1.26	26.14	55.89	-	7.68	7.94	0.26	0.29	27.94

2.1.7 Mineralogical analysis of Manki soil sample

As per quantification of results from Figure 7(d), it is found that the soil sample consists of relatively greater percentage of magnesium-based compounds like vermiculite (13.9%) and biotite (11.9%) and also signifies the presence of microcline (8.9%), gibbsite (8.9%), illite (7.9%) and mullite (7.9 %) at relatively higher proportions. The quartz (2%), dozyite (2%), alumina (1%), forsterite (1%) and iron oxide (1%) are found in low percentages. The SEM image of Figure 7(a) also confirms the presence of layered structure having magnesium-based compounds like biotite and vermiculite as observed by Ozgurluk *et al*., [23].

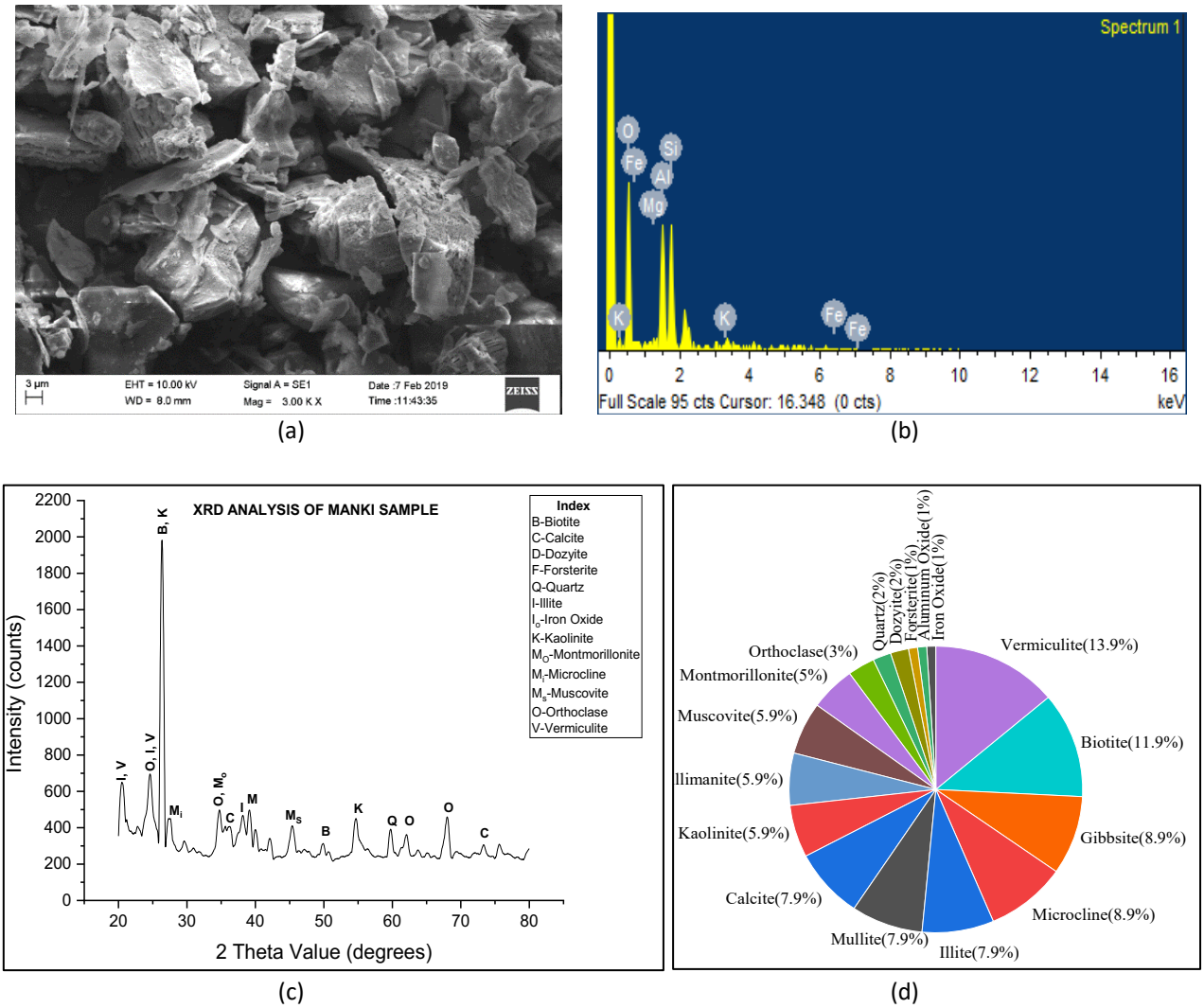

Fig. 7. Manki sample (a) SEM image (b) Spectrum image (c) XRD analysis (d) Quantification of compounds

The minerals in the XRD analysis as in Figure 7(c) are evident from the elements witnessed by the EDS analysis as listed in the Table 7. Most of the elements observed are oxygen, silicates and aluminium followed by potassium, iron and magnesium as depicted by spectrum image in Figure 7(b). Vermiculites are weathered products of biotite. The presence of both biotite and vermiculite compounds confirms their presence through a clear peak intensity. The main elements of these compounds like aluminium, silica, iron, and magnesium are clearly evident from the EDS analysis as shown in Table 7.

Table 7
Elemental composition of Manki sample

Elements	O	Mg	Al	Si	K	Fe	O	Mg	Al	Si	K	Fe
	Weight (%)						Atomic Weight (%)					
Spectrum 1	51.69	0.54	18.31	25.15	2.85	1.46	65.58	0.45	13.78	18.18	1.48	0.53
Spectrum 2	55.27	0.4	21.63	19.72	1.23	1.74	68.58	0.32	15.91	13.94	0.63	0.62

2.1.8 Mineralogical analysis of Honnavar soil sample

As per quantification of results from Figure 8(d), the soil sample contains larger proportions of biotite (18.8%) followed by microcline (15.8%), montmorillonite (13.9%) and gibbsite (6.9%). The quartz (1%), alumina (1%), forsterite (1%) and iron oxide (1%) are present at very small proportions. The montmorillonite is found to be at 13.9 % of total volume, which is relatively high among other soil samples. The SEM image as per Figure 8(a) can be recognized as fibrous Illite [20]. The compounds identified in the XRD analysis are confirmed through elements observed by the EDS analysis as listed in Table 8. Most of the elements observed from spectrum image as in Figure 8(b) are oxygen, silicates and aluminium followed by potassium, iron, and carbon.

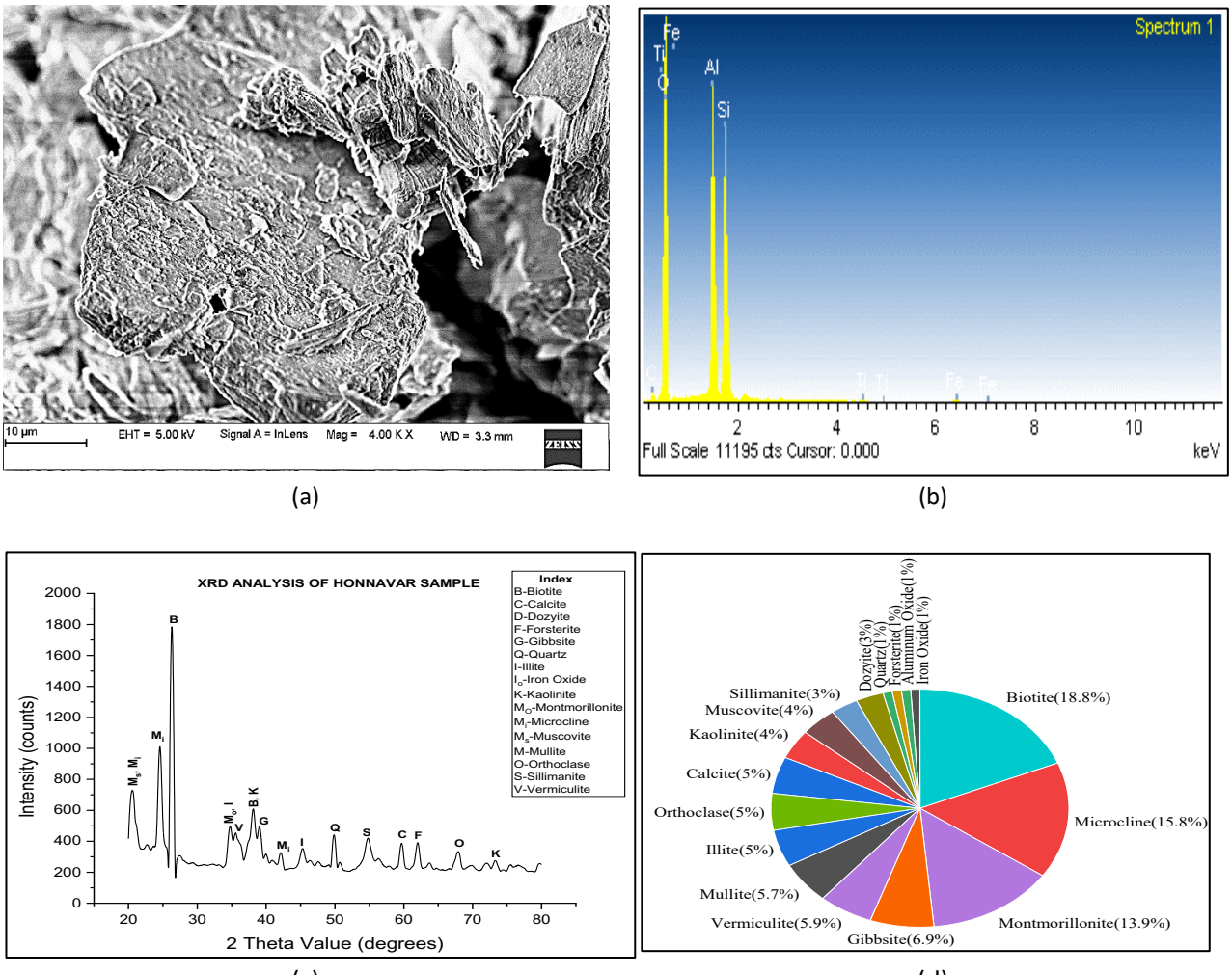

(a) (b)

(c) (d)

Fig. 8. Honnavar sample (a) SEM image (b) Spectrum image (c) XRD analysis (d) Quantification of compounds

The microcline, quartz, Illite, kaolinite, sillimanite minerals can be observed in the peaks shown by XRD analysis in Figure 8(c). The elements depicted in EDS analysis reveals the presence of potassium, aluminium, iron and silicate-based compounds like microcline, gibbsite, orthoclase, muscovite and magnesium-based compounds are not witnessed by EDS analysis as presence of magnesium is not detected by EDS analysis.

Table 8
Elemental composition of Honnavar sample

Elements	O	Al	Si	K	Ti	Fe	C	O	Al	Si	K	Ti	Fe	C
	Weight (%)							Atomic Weight (%)						
Spectrum 1	56.95	12.57	16.27	0.75	-	2.51	21.38	55.2	7.22	8.98	0.3	-	0.7	27.6
Spectrum 2	115.8	26.71	27.64	-	0.48	1.99	43.47	56.21	7.69	7.64	-	0.08	0.28	28.11

2.1.9 Mineralogical analysis of Haladipur soil sample

The figure showing SEM image in Figure 9(a), can be considered as sheet structured mineral vermiculite [23]. As per quantification of results from Figure 9(d), the soil sample consists of relatively larger proportions of illite (18%) and muscovite (17%) followed by microcline (13%), biotite (7%) and vermiculite (7%). The quartz (3%), alumina (3%), forsterite (1%) and mullite (1%) are present at lesser percentages. The compounds observed in the XRD analysis as in Figure 9(c) are evident from the elements observed by the EDS analysis as listed in Table 9 and as depicted in spectrum image Figure 9(b). Most of the elements observed are oxygen, silicates, aluminium, iron, magnesium and potassium.

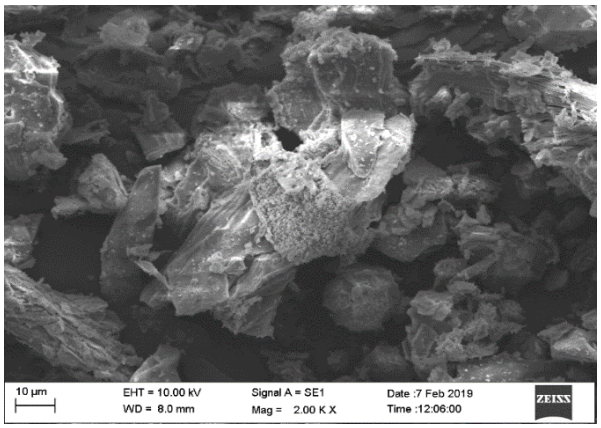

(a)

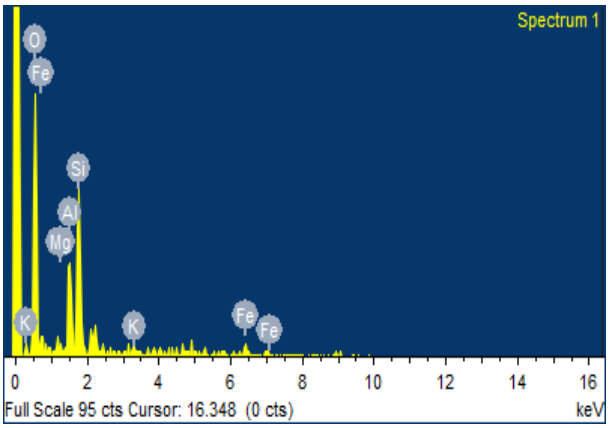

(b)

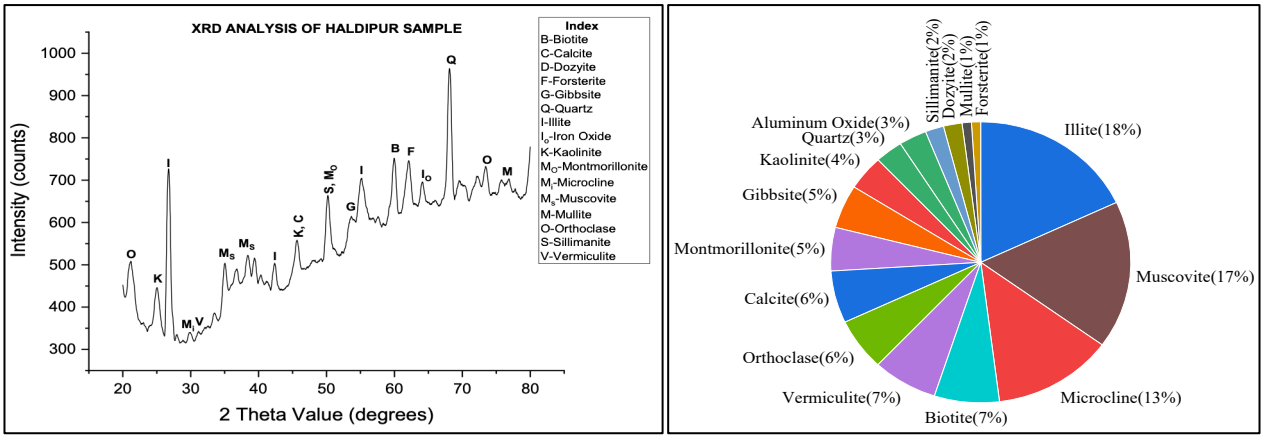

(c) (d)

Fig. 9. Haladipur sample (a) SEM image (b) Spectrum image (c) XRD analysis (d) Quantification of compounds

The illite, muscovite, microcline, quartz, biotite, kaolinite, sillimanite, montmorillonite, and vermiculite minerals are evident from the peaks shown by XRD analysis as shown in Figure 9(c). The elements depicted by EDS analysis as in Figure 9(b) reveals the presence of potassium, aluminium, iron and silicate-based compounds like illite, muscovite, microcline, gibbsite, orthoclase, muscovite and magnesium-based compounds like biotite, vermiculite and dozyite are witnessed by the presence of magnesium in the EDS analysis.

Table 9
Elemental composition of Haladipur sample

Elements	O	Mg	Al	Si	K	Fe	O	Mg	Al	Si	K	Fe
Weight (%)							Atomic Weight (%)					
Spectrum 1	55.22	0.34	14	21.72	2.67	6.05	69.95	0.28	10.52	15.67	1.38	2.2
Spectrum 2	52.66	0.19	11.57	24.63	0.55	10.39	68.5	0.17	8.92	18.25	0.29	3.87

2.1.10 Mineralogical analysis of Kumta soil sample

The SEM image as in Figure 10(a) confirms the presence of layered kaolinite. As per quantification of result, from Figure 10(d), the soil sample contains relatively larger proportions of vermiculite (12.7%), microcline (10.8%), illite (9.8%) and kaolinite (9.8%). The quartz (1%), sillimanite (2%), alumina (2.9%), forsterite (2.8%) and albite (1%) are present at lower percentages.

The minerals noted in the XRD analysis as in Figure 10(c) are evident from the elements depicted by the EDS analysis as listed in Table 10. Most of the elements observed are oxygen, silicates, aluminium, iron, potassium, sodium and calcium. The kaolinite, microcline, Illite, quartz, biotite, montmorillonite, muscovite, orthoclase and vermiculite minerals can be observed in the peaks shown by XRD analysis. The elements identified in EDS analysis in Figure 10(b) confirms the presence of aluminium, silicate, potassium, aluminium, iron, based compounds like illite, muscovite, microcline, gibbsite, orthoclase and sodium-based compound like albite is witnessed by the presence of sodium in the EDS analysis. The calcite is witnessed by the presence of calcium in the EDS analysis.

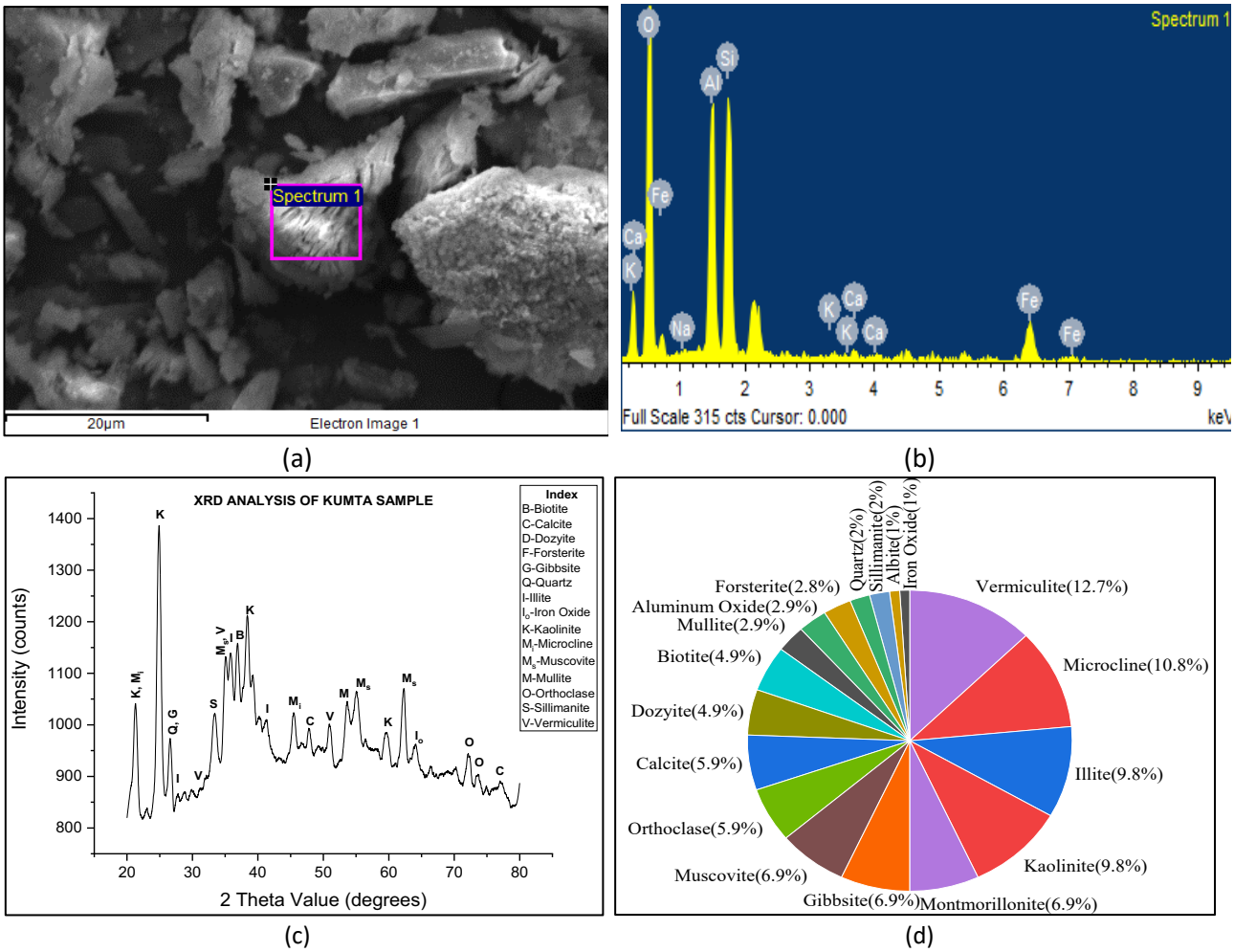

Fig. 10. Kumta sample (a) SEM image (b) Spectrum image (c) XRD analysis (d) Quantification of compounds

Feldspar, constituting over 50% of the Earth's surface, is a silicate mineral integral to various geological components. It is present in igneous, metamorphic, and sedimentary rocks across the field. Feldspars, including orthoclase ($KAlSi_3O_8$), are found in diverse geological formations.

Illite-type clays, conversely, develop in conditions of increased pH as a result of the weathering of potassium (K) and aluminium (Al) rich rocks. Their formation involves the modification of minerals like muscovite and feldspar. In the soil sample, shales are predominantly composed of Illite clays. Illite encompasses a diverse category of mica, characterized as 2:1 layer minerals, such as micas and montmorillonites, where one octahedral unit is surrounded by two silica tetrahedra units. Notably, Illites exhibit variations from mica minerals in several aspects: approximately one-sixth of the Si^{4+} ions in illites are substituted by Al^{3+} ions, whereas in regular micas, one-fourth of the Si4+ ions undergo substitution; additionally, illites have a lesser cation deficiency. The interface position in illites adsorbs a lower amount of potassium. Illite particles are typically small, measuring less than 1 to 2 microns, which can be attributed to the weaker bonding of K^+ in the interface positions. Clay minerals, notably montmorillonite, demonstrate a noticeable adsorption capacity. The chemical adsorption of potassium ions by montmorillonite can result in the creation of illite. These minerals are frequently present in igneous and metamorphic rocks. Potash feldspar is more commonly encountered in the form of microcline rather than as orthoclase [24]. The muscovite, phlogopite, biotite, and chlorite indicate that the water appears to serve as a lubricant in sheet minerals. This is due to the thin adsorbed coating and partially hydrated surface ions in air. As a result, the adsorbed layer is difficult to disturb. The increased thickness of the surface films as well as the increased surface

ion hydration and dissociation increase their mobility when the surfaces of layer silicates are moist [25].

Table 10
Elemental composition of Kumta sample

Elements	O	Na	Al	Si	K	Ca	Fe	O	Na	Al	Si	K	Ca	Fe
Weight (%)								Atomic Weight (%)						
Spectrum 1	51.51	0.1	18.58	20.87	0.19	-	8.75	66.83	0.09	14.3	15.42	0.1	-	3.25
Spectrum 2	50.23	0.25	14.41	18.26	0.28	0.78	15.8	67.6	0.23	11.5	14	0.15	0.42	6.09

4. Conclusion

The soil samples gathered from different locations encompass both primary and secondary minerals. Predominantly, the primary minerals identified in most locations include unchanged constituents such as quartz, feldspar (including orthoclase, microcline, albite), and mica group minerals like muscovite and biotite, which have maintained their chemical composition since their initial formation. The secondary minerals, resulting from the decomposition and chemical transformation of primary minerals, consist of kaolinite, illite, montmorillonite, vermiculite, gibbsite, and calcite. The samples exhibit a blend of these minerals in varying proportions.

The common elements present in all site locations as per EDS analysis are Si, Al, Fe, O, K. The Kumta sample shows the presence of Na and Ca in addition to common minerals. The Honnavar sample shows presence of Titanium in addition. The Magnesium is present in all the soil samples except samples of Shirali, Honnavar and Kumta. The presence of Mg confirms the presence of vermiculite and biotite minerals. The proportion of microcline mineral varies from 8.9 to 21% and is common mineral found at all the locations. Some other minerals such as muscovite varies from 4% to 17%, gibbsite varies from 3.1 to 13.9%, quartz varies from 1 to 5%, Illite varies from 5 to 18%.

Acknowledgement
This research was not funded by any grant.

References
[1] Thomas, Biji Chinnamma, R. Shivashankar, Sarah Jacob, and Meera Susan Varghese. "Erosion studies on lithomargic clays." *Indian Geotechnical Journal* 50, no. 1 (2020): 142-156. https://doi.org/10.1007/s40098-019-00364-8
[2] Nayak, Sitaram, and Purushotham G. Sarvade. "Effect of cement and quarry dust on shear strength and hydraulic characteristics of lithomargic clay." *Geotechnical and Geological Engineering* 30 (2012): 419-430. https://doi.org/10.1007/s10706-011-9477-y
[3] Varghese, George, Hegde Ramakrishna, AG Nirmal Kumar, L. Durga Prashanth, and G. Santosh. "A Model Study on Accelerated Consolidation of Coir Reinforced Lateritic Lithomarge Soil Blends with Vertical Sand Drains for Pavement Foundations." *Open Journal of Soil Science* 2, no. 03 (2012): 320. https://doi.org/10.4236/ojss.2012.23038
[4] Nayak, Deepak, Purushotham G. Sarvade, Udaya Shankara HN, and Jagadeesha B. Pai. "Mineralogical Characterization of Lithomargic Clay Deposits along the Coastal Belt of Udupi Region of South India." *Journal of Composites Science* 7, no. 4 (2023): 170. https://doi.org/10.3390/jcs7040170
[5] Shivashankar, R., Biji Chinnamma Thomas, K. T. Krishnanunni, and D. Venkat Reddy. "Slope stability studies of excavated slopes in lateritic formations." In *Geotechnical Applications: IGC 2016 Volume 4*, pp. 127-134. Springer Singapore, 2019. https://doi.org/10.1007/978-981-13-0368-5_14
[6] Linda, J., and V. Rani. "Dispersive Characteristics of Soils." *Int. J. Res. Eng. Sci. Manag* 3 (2020): 467-469.
[7] Sarvade, Purushotham G., Deepak Nayak, Aayush Sharma, Ragini Gogoi, and Sagar Madhukar. "Strength characteristics of Randomly distributed coconut coir Reinforced lithomargic clay." *International Journal of Civil Engineering and Technology* 8, no. 5 (2017): 1122-1134.

[8] Sarvade, Purushotham G., Deepak Nayak, Aayush Sharma, Ragini Gogoi, and Sagar Madhukar. "Evaluation of strength chacteristics of coconut coir mat reinforced lithomargic clay." *International Journal of Civil Engineering and Technology* 9, no. 8 (2018): 1168-1179.
[9] Budihal, Rajendrakumar, and Ganapathi Pujar. "Major and trace elements geochemistry of laterites from the Swarnagadde plateau, uttar Kannada district, Karnataka, India." *J. Geosci. Geomat* 6, no. 1 (2018): 12-20.
[10] Sekhar, Darshan C., and Sitaram Nayak. "SEM and XRD investigations on lithomargic clay stabilized using granulated blast furnace slag and cement." *International Journal of Geotechnical Engineering* (2017). https://doi.org/10.1080/19386362.2017.1380355
[11] Momade, F. W. Y., and S. K. Y. Gawu. "Geochemical and mineralogical characteristics of lithomargic clay types from Awaso bauxite deposit, Ghana: implications for possible industrial utilization." *Journal of Science and Technology (Ghana)* 29, no. 2 (2009). https://doi.org/10.4314/just.v29i2.46227
[12] Laita, Elisa, Blanca Bauluz, María José Mayayo, and Alfonso Yuste. "Mineral and textural transformations in mixtures of Al-rich and Al–K-rich clays with firing: Refractory potential of the fired products." *Ceramics International* 47, no. 10 (2021): 14527-14539. https://doi.org/10.1016/j.ceramint.2021.02.032
[13] Mahesh Bhat, K., and Sitaram Nayak. "Experimental studies and its application using PLAXIS-2D for lithomargic clay stabilized by GBFS and lime." *Geotechnical and Geological Engineering* 39 (2021): 4901-4915. https://doi.org/10.1007/s10706-021-01802-2
[14] Narloch, Piotr, Piotr Woyciechowski, Jakub Kotowski, Ireneusz Gawriuczenkow, and Emilia Wójcik. "The effect of soil mineral composition on the compressive strength of cement stabilized rammed earth." *Materials* 13, no. 2 (2020): 324. https://doi.org/10.3390/ma13020324
[15] Amulya, S., A. U. Ravi Shankar, and Medari Praveen. "Stabilisation of lithomargic clay using alkali activated fly ash and ground granulated blast furnace slag." *International Journal of Pavement Engineering* 21, no. 9 (2020): 1114-1121. https://doi.org/10.1080/10298436.2018.1521520
[16] Sarvade, Purushotham G., and Sitaram Nayak. "Microfabric and mineralogical studies using sem and xrd on the lithomargic clay stabilized with cement and quarry dust." *International Journal of Earth Sciences and Engineering* 4, no. 5 (2015): 266-273.
[17] Bhagyashree, H. N. Udayashankar, Purushotham Sarvade, Kavyashree, "Correlation of Mineralogical and Geotechnical Properties of Laterite Soils of Coastal Karnataka, India," *Civil Engineering and Architecture, Vol. 11, No. 6, pp. 3334 - 3346*, (2023). https://doi.org/10.13189/cea.2023.110609
[18] Sarga Manoj, Soorya S R. "A Review on Variation of The Geotechnical Properties of Lithomargic Clay Subjected to Contamination." *International journal of engineering research & technology (ijert), Volume 10, Issue 06*, (2022).
[19] Sruthi, P. Lakshmi. "Characterization of kaolinitic clays subjected to alkali contamination." *Applied Clay Science* 146 (2017): 535-547. https://doi.org/10.1016/j.clay.2017.07.012
[20] Peltz, Markus, Arne Jacob, Georg H. Grathoff, Frieder Enzmann, Michael Kersten, and Laurence N. Warr. "A FIB-SEM study of Illite morphology in Aeolian Rotliegend Sandstones: implications for understanding the petrophysical properties of reservoir rocks." *Clays and Clay Minerals* 70, no. 1 (2022): 84-105. https://doi.org/10.1007/s42860-022-00174-9
[21] Suzuki, Tasuma, Akira Nakamura, Masakazu Niinae, Hideki Nakata, Hiroshi Fujii, and Yukio Tasaka. "Lead immobilization in artificially contaminated kaolinite using magnesium oxide-based materials: Immobilization mechanisms and long-term evaluation." *Chemical engineering journal* 232 (2013): 380-387. https://doi.org/10.1016/j.cej.2013.07.121
[22] Kalita, J. M., and G. Wary. "Effect on thermoluminescence parameters of biotite mineral due to thermal quenching." *Journal of luminescence* 132, no. 11 (2012): 2952-2956. https://doi.org/10.1016/j.jlumin.2012.06.009
[23] Ozgurluk, Yasin, Kadir Mert Doleker, Hayrettin Ahlatci, Dervis Ozkan, and Abdullah Cahit Karaoglanli. "The microstructural investigation of vermiculite-infiltrated electron beam physical vapor deposition thermal barrier coatings." *Open Chemistry* 16, no. 1 (2018): 1106-1110. https://doi.org/10.1515/chem-2018-0097
[24] Brian, Mason, and B. M. Carleton. "Principles of Geochemistry." (1982).
[25] Mitchell, James Kenneth, and Kenichi Soga. *Fundamentals of soil behavior*. Vol. 3. New York: John Wiley & Sons, 2005.